JOURNAL OF THE GEOTECHNICAL ENGINEERING DIVISION

SITE FACTORS CONTROLLING LIQUEFACTION

By Rafael M. Blázquez,[1] Raymond J. Krizek,[2] M. ASCE, and Zdeněk P. Bažant,[3] M. ASCE

INTRODUCTION

Developed herein is a one-dimensional model to analyze liquefaction of a sand layer due to the upward propagation of shear and pressure waves from the base. A nonlinear endochronic constitutive law (8) is utilized in conjunction with an inelastic two-phase medium framework (2) to represent the mechanical behavior of saturated sands. By so doing the pore-pressure buildup is obtained directly from the constitutive equation and the solution of the boundary value problem. Thus, there is no need to introduce the pore-pressure buildup separately in the general formulation. The same consideration applies to viscous damping, which is expressed in the equations of motion for the system by a term assigning a specified resistance to the flow of water through the pore channels of the soil skeleton (Darcy's law) for those cases in which perfect coupling between phases does not occur. This viscous damping is in addition to the hysteretic damping that emanates from the constitutive equation itself and reflects a completely different physical mechanism (namely, Coulomb friction between grains). In this work the endochronic liquefaction model is applied to various typical field situations and the effect of various factors presumed to govern field liquefaction phenomena is evaluated.

ONE-DIMENSIONAL MODEL FOR DYNAMIC PORE PRESSURE BUILD-UP

Consider a stratum of inelastic saturated sand, infinitely long in the horizontal direction, resting on a rigid nonsloping bedrock. Within the context of a two-phase

Note.—Discussion open until December 1, 1980. To extend the closing date one month, a written request must be filed with the Manager of Technical and Professional Publications, ASCE. This paper is part of the copyrighted Journal of the Geotechnical Engineering Division, Proceedings of the American Society of Civil Engineers, Vol. 106, No. GT7, July, 1980. Manuscript was submitted for review for possible publication on April 9, 1979.

[1] Laboratorio Nacional del Transporte y Mecanica del Suelo, Madrid, Spain; formerly, Graduate Student, Northwestern Univ., Evanston, Ill.
[2] Prof. of Civ. Engrg., Northwestern Univ., Evanston, Ill.
[3] Prof. of Civ. Engrg., Northwestern Univ., Evanston, Ill.

medium approach for isotropic materials, the volumetric constitutive equations of the confined sand may be formulated in differential form as (2)

$$d\sigma = M(d\epsilon - d\epsilon'') + Q(d\epsilon_F - d\epsilon''_F) \quad \ldots\ldots\ldots\ldots\ldots\ldots\ldots\ldots (1a)$$

$$d\sigma_F = Q(d\epsilon - d\epsilon'') + R(d\epsilon_F - d\epsilon''_F) \quad \ldots\ldots\ldots\ldots\ldots\ldots\ldots\ldots (1b)$$

in which $\sigma = \sigma' - (1 - n)\, p_w$ and $\sigma_F = -np_w$ are the stresses in the solid and fluid phases, respectively (σ' = effective stress and p_w = pore water pressure); M = the tangent constrained modulus of the solid skeleton; R = the bulk modulus of the fluid phase; and Q = a coupling coefficient that is given by $(1 - n)/C_w$ (n = porosity and C_w = compressibility of fluid). The terms $d\epsilon''$ and $d\epsilon''_F$ represent incremental inelastic (irrecoverable) strains that depend on the process of loading to which the soil is subjected. In particular, for liquefaction phenomena $d\epsilon''$ represents the increment of densification of the sand due to the slip of grains and the subsequent rearrangement of particles into denser configurations. For simple shear conditions $d\epsilon''$ can be expressed as (8)

$$d\epsilon'' = -\frac{d\kappa}{c(\kappa)}; \quad c(\kappa) = 1 + \alpha\kappa \quad \ldots\ldots\ldots\ldots\ldots\ldots\ldots\ldots (2a)$$

$$d\kappa = F[J_2(e_{ij})]\, d\xi = \frac{q}{4} |\gamma|^{q-1} |d\gamma| \quad \ldots\ldots\ldots\ldots\ldots\ldots\ldots\ldots (2b)$$

in which κ = densification measure; $c(\kappa)$ = densification-hardening function; ξ = rearrangement measure; F = strain-softening function; $J_2(e_{ij})$ = second invariant of the deviator of the strain tensor; γ = shear angle; and q and α = material parameters that depend on the initial relative density of the sand. The endochronic shear stress-shear strain relationship for the solid skeleton (the fluid is assumed incapable of resisting shear strains) can be written as (3)

$$de_{ij} = \frac{ds_{ij}}{2G} + de''_{ij}; \quad de''_{ij} = \frac{s_{ij}}{2G}\frac{d\zeta}{Z_1} \quad \ldots\ldots\ldots\ldots\ldots\ldots\ldots\ldots (3)$$

in which G = shear modulus; s_{ij} = deviator of the stress tensor; e_{ij} = deviator of the strain tensor; e''_{ij} = inelastic shear strain; ζ = intrinsic time; and Z_1 = "relaxation" constant. For the special case of a one-dimensional simple shear stress, τ, Eq. 3 becomes

$$d\tau = G(d\gamma - d\gamma'') = G\left(d\gamma - \frac{\tau}{G}\frac{d\zeta}{Z_1}\right) \quad \ldots\ldots\ldots\ldots\ldots\ldots\ldots\ldots (4)$$

in which $\gamma'' = 2e''_{12}$ = inelastic shear angle. Eqs. 1a, 1b, and 4 fully characterize the nonlinear behavior of a stratum of sand subjected to arbitrary loading conditions. Thus, the dynamic response of the layer can be determined if the previous equations are combined with the equations of motion for a porous medium infinitely long in the horizontal direction and saturated with a viscous fluid, namely (5)

$$\frac{\partial\sigma}{\partial y} = (\rho_1 + \rho_a)\frac{\partial^2 u}{\partial t^2} - \rho_a\frac{\partial^2 U}{\partial t^2} + b\left(\frac{\partial u}{\partial t} - \frac{\partial U}{\partial t}\right) - \rho_1 g \quad \ldots\ldots\ldots\ldots (5a)$$

$$\frac{\partial \sigma_F}{\partial y} = -\rho_a \frac{\partial^2 u}{\partial t^2} + (\rho_2 + \rho_a)\frac{\partial^2 U}{\partial t^2} - b\left(\frac{\partial u}{\partial t} - \frac{\partial U}{\partial t}\right) - \rho_2 g \quad \ldots\ldots\ldots (5b)$$

$$\frac{\partial \tau}{\partial y} = (\rho_1 + \rho_2)\frac{\partial^2 v}{\partial t^2} \quad \ldots\ldots\ldots\ldots\ldots\ldots\ldots\ldots\ldots\ldots\ldots\ldots (5c)$$

in which u and U = vertical displacements of the solid and the fluid, respectively; v designates the horizontal displacements (assumed to be equal for both phases throughout the entire history of motion); ρ_1 and ρ_2 = the mass densities of the solid and fluid phases; g = the acceleration of gravity; and ρ_a and b = the dynamic coupling parameters, termed apparent coupled mass density and flow resistance coefficient, respectively. The liquefaction model is then given by Eqs. 4 and 5c for the deviatoric response and Eqs. 1a, 1b, 5a and 5b for the volumetric response.

If it is assumed that the vertical displacements of the grains and the water are equal everywhere within the mass ($u = U$), the total deformations of the solid, $d\epsilon$, and the fluid, $d\epsilon_F$, must be equal (because the volumetric strains are the divergences of the corresponding displacement fields), and no seepage occurs (this is true for a sufficiently short time period after load application). Moreover, if it can be further assumed that the total vertical stress remains constant with time—as occurs in the field when the overburden of a given soil element is constant ($d\sigma = -d\sigma_F$)—and the compressibility of the water is negligible relative to that of the skeleton, Eqs. 1 yield:

$$dp_w^g = -\frac{d\epsilon''}{C_d} \quad \ldots\ldots\ldots\ldots\ldots\ldots\ldots\ldots\ldots\ldots\ldots\ldots\ldots\ldots (6)$$

in which superscript g indicates "generated pore pressure"; and the coefficient C_d, termed the "densification compliance," is simply the drained confined compressibility of the sand (2). Eq. 6 is the simplest equation that is able to characterize the pore-pressure increase due to densification in undrained sand; a similar relationship has been derived by others (14,16) using a different approach.

If drainage occurs during shaking, Eq. 6 does not give the actual pressures, because the seepage of water through the pores of the skeleton will reduce the rate of pore-pressure buildup. However, Eq. 6 still gives correct pressure increments for infinitely short time intervals. If all of the assumptions of Terzaghi's simplified theory of consolidation (20) hold and if the inelastic strains have a negligible effect on the permeability and recovery stiffness, the distribution of pore water pressure at time t is controlled by (9)

$$\frac{\partial p_w}{\partial t} = \frac{\partial}{\partial y}\left(\frac{k}{\gamma_w C_d}\frac{\partial p_w}{\partial y}\right) + \frac{1}{C_d}\frac{\partial \epsilon''}{\partial t} \quad \ldots\ldots\ldots\ldots\ldots\ldots\ldots\ldots\ldots (7)$$

in which k = the coefficient of permeability of the soil; and γ_w = the unit weight of water. Eq. 7 governs the redistribution of pore pressures that takes place in the deposit. Thus, the evaluation of the liquefaction susceptibility of a drained sand deposit leads to solving a problem of consolidation with internal pore-pressure generation.

Analytical Estimates of Pore Pressure

If the problem can be simplified to one involving a homogeneous layer with constant recovery properties (C_d = constant), an analytical solution for the governing equation

$$\frac{\partial p_w}{\partial t} = c_v \frac{\partial^2 p_w}{\partial y^2} + \frac{\partial p_w^g}{\partial t}; \quad c_v = \frac{k}{\gamma_w C_d} \quad \ldots\ldots\ldots\ldots\ldots\ldots\ldots\ldots (8)$$

exists and can be found by superposition. Thus, if the excess pore pressure is uniform with depth and varies linearly with time, the solution of Eq. 8 for

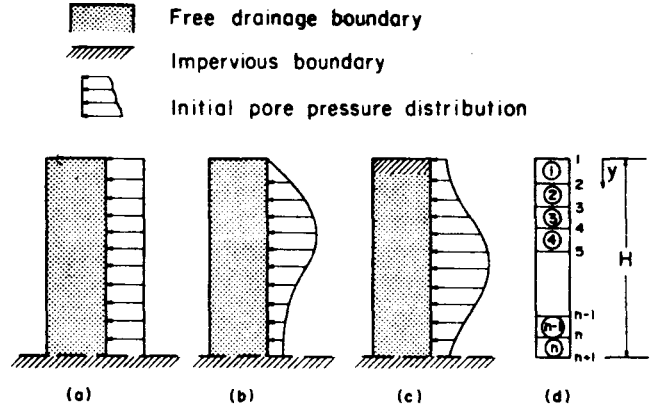

FIG. 1.—Different Boundary and Initial Conditions for Discretized Sand Layer

the boundary and initial conditions shown in Fig. 1(a) is obtained by applying the convolution integral (7)

$$p_w(y,t) = p_w^g(0)A(y,t) + \int_0^t A(y,t-\tau)\left(\frac{\partial p_w^g}{\partial t}\right)_{t=\tau} d\tau \quad \ldots\ldots\ldots\ldots (9)$$

in which $p_w^g(0) = 0$ and $A(y,t)$ is the compliance function of the deposit:

$$A(y,t) = \sum_{n=1}^{\infty} \frac{2(1-\cos n\pi)}{n\pi} \sin\frac{n\pi y}{2H} \exp\left(\frac{-n^2\pi^2 c_v t}{4H^2}\right) \quad \ldots\ldots\ldots\ldots (10)$$

that is, the excess pore pressure generated in the layer when acted upon by a value of p_w^g equal to unity. Specifically, for a linear increase in pore water pressure $p_w^g = \beta t$, substitution of Eq. 10 into Eq. 9 and integration with respect to time gives

$$p_w(y,t) = \frac{8\beta}{\pi^3}\sum_{n=1}^{\infty}\frac{1}{n^3}(1-\cos n\pi)\sin\frac{n\pi y}{2H}\left[1-\exp\left(\frac{-n^2\pi^2 c_v t}{4H^2}\right)\right] \quad (11)$$

whereas for an arbitrary monotonic increase of p_w^g with time, we obtain (for uniform and time-constant properties of the layer)

$$p_w(y,t) = \sum_{\tau=0} \text{Rel}\,(dp^g_w)_{t-\tau} \quad \ldots \quad (12)$$

in which the operation Rel ( ) indicates the relaxation for time t of a unit increment of the pore pressure generated at the instant $t = \tau$ [obviously the function $A(y,t)$ lacks meaning in this case, since the magnitude of $p^g_w(t)$ varies with position within the profile].

For a top-draining stratum [Fig. 1(*b*)], the initial values of the pore-pressure increments developed due to the densification of undrained sand are given by

$$dp_w(H-y,t) = \frac{2}{H}\sum_{n=0}^{\infty} \exp\left[\frac{-c_v(n+1)^2\pi^2 t}{4H^2}\right] \sin\frac{(2n+1)\,\pi\,(H-y)}{2H}$$

$$\int_0^H [dp^g_w(H-y)]_{t=\tau} \sin\frac{(2n+1)\,\pi\,(H-y)}{2H}\,dy \quad \ldots \quad (13)$$

while for a sealed stratum (Fig. 1*c*), we have

$$dp_w(y,t) = \frac{1}{H}\int_0^H [dp^g_w(y)]_{t=\tau}\,dy$$

$$+ \frac{2}{H}\sum_{n=1}^{\infty} \exp\left[\frac{-c_v n^2\pi^2 t}{H^2}\right] \cos\frac{n\pi y}{H} \int_0^H [dp^g_w(y)]_{t=\tau} \cos\frac{n\pi y}{H}\,dy \quad \ldots \quad (14)$$

Eqs. (13) and (14) are formally analogous to the solutions of the heat conduction equation for a bar of length H with one or two ends insulated, respectively, in which an infinitesimal distribution of initial temperature, $dp^g_w(y)$, is prescribed at time $t = \tau$ (6). Although these relations are only approximate because the convolution integral is replaced by a summation formula, they can deal with: (1) Redistribution effects (Eq. 11 can not); (2) any type of external boundary conditions; (3) arbitrary shapes of the initial isochrones; and (4) nonlinear histories of generated pore pressures. The present superposition method may be applied to a series of initial value problems; this constitutes a somewhat limited, but useful, alternative approach to the direct solution of the differential equation given by Eq. 7.

Finite Element Solution

The final step in the calculation is the step-by-step integration in time ($\Delta\tau = 0.01$ sec) of the nonlinear differential equations that result from solving the deviatoric and (eventually) the volumetric responses. This was accomplished by using the implicit Newmark β-method (with $\beta = 0.25$ and $\alpha = 0.5$); for this particular nonlinear problem, this integration method is unconditionally stable and has no spurious damping (4). Various typical cases have been solved to evaluate the effect of different parameters in the mathematical model and their influence on field liquefaction.

Review of Factors Governing Liquefaction Phenomena

Virtually all experimental investigations have confirmed the fact that the resistance of a given sand to liquefaction is strongly influenced by its grain

size distribution, initial relative density, initial effective stress, amplitude of excitation, and duration of loading, but not significantly by its grain size or roundness or the mineralogical composition of its particles (12,13,18). For field situations additional controlling factors are: (1) Shear resistance of overburden; (2) drainage; (3) compressibility of soil; (4) layer thickness; (5) characteristics of input motion; and (6) degree of dynamic coupling. The effects of these parameters have been studied using the present endochronic liquefaction model and the results have been compared with the findings of others to establish general trends.

Effect of Shear Resistance of Overburden.—In analytical studies of liquefaction the water table is commonly regarded as a nondraining surface, and the overlying

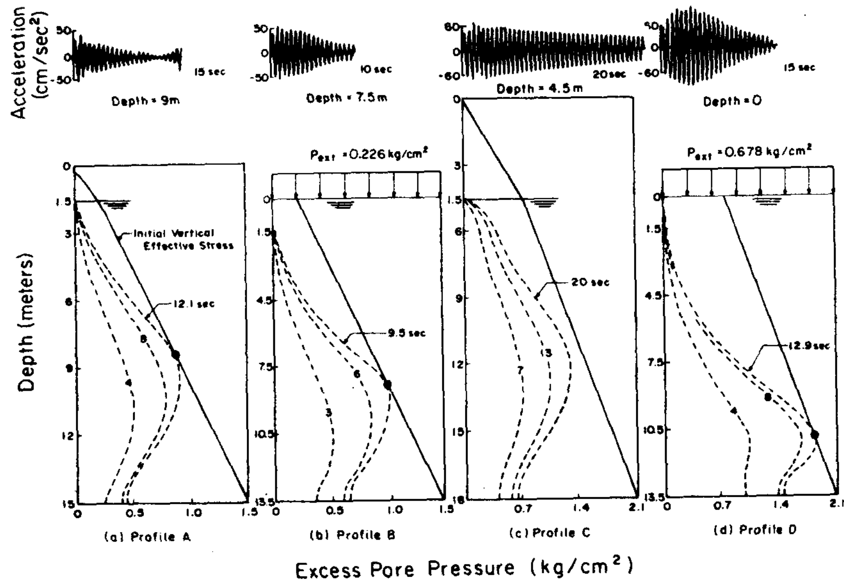

FIG. 2.—Computed Accelerations and Development of Excess Pore Water Pressures in Liquefying Layers Subjected to Cyclic Loading

soil is assumed to be either completely dry (no capillary effects) or replaced by a rigid frictionless slab having the same weight as the dry soil. To examine the influence of this assumption within the framework of the endochronic liquefaction model, a 15-m deep layer of saturated Crystal Silica No. 20 sand with a relative density of 60% was subjected to harmonic loading. The dry unit weight of the sand was taken as 1.49 g/cm^3, and the water table was located 1.5 m below the ground surface. For purposes of calculation, the column of soil was divided into 10 equal intervals of 1.5 m each [$n = 10$ in Fig. 1(*d*)]; the bedrock underlying the deposit was assumed to be rigid and to accelerate sinusoidally in a horizontal direction with a frequency of 2 Hz and an amplitude of 0.0325 *g*. The acceleration histories for the liquefied elements and the pore pressure development up to initial liquefaction are shown in Figs. 2(*a*) and

2(*b*). The computed accelerations are seen to decrease slowly until they become very small (this is due to the inability of the soil to transmit shear waves after the onset of liquefaction) at times of 12.1 sec and 9.5 sec for the unsaturated and saturated profiles, respectively. Since undrained conditions are assumed in the calculations, this point is mathematically defined as that where the isochrone of the excess pore water pressure becomes tangent to the initial effective stress line.

Two additional profiles were studied by using the same acceleration input and a water table depth three times larger (4.5 m) to evaluate the effect of replacing the dry soil cover by a dead weight. The computed results presented in Figs. 2(*c*) and 2(*d*) show that the amplification of the bedrock acceleration at the elevation of the water table is 25% greater for the case of the surcharge

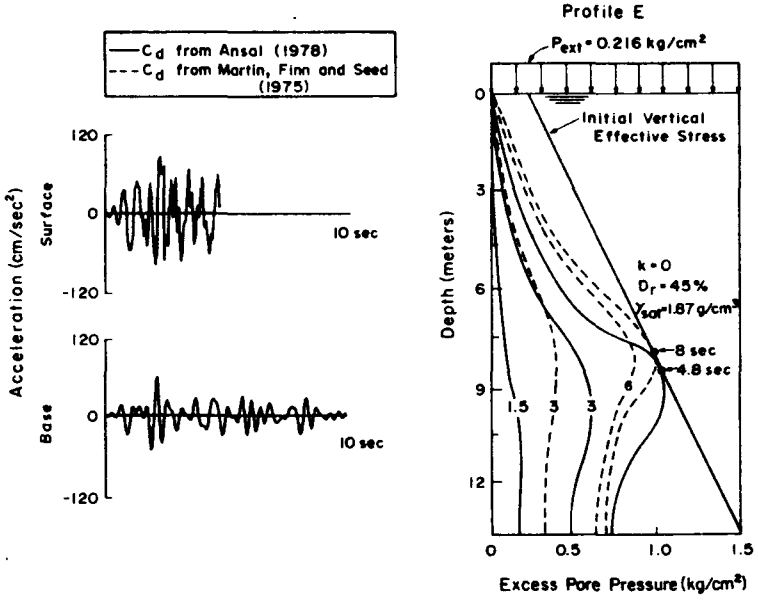

FIG. 3.—Acceleration Response and Effect of Soil Compressibility on Liquefaction of Undrained Layer Subjected to Synthetic Accelerogram

relative to the unsaturated profile. In addition, the latter does not liquefy in 20 sec, whereas the former reaches the liquefied state at a depth of about 11.2 m after 12.9 sec of cyclic loading. Thus, even in the absence of vertical inertial effects, the rigid slab approximation can only be accepted within a reasonable degree of accuracy for small values of the ratio of the water table depth to the thickness of the layer. In addition, the potential benefit of preloading the deposit to avoid liquefaction becomes evident by simply comparing Figs. 2(*a*) and 2(*b*) with Figs. 2(*c*) and 2(*d*).

Effect of Drainage.—By applying the superposition method (Eq. 9), Christian (7) concluded that, for all practical purposes, if the pore pressures are assumed to rise linearly during liquefaction, no simultaneous dissipation by consolidation

takes place in the layer unless very large transition times are considered. This conclusion seemingly contradicts the results computed from Eq. 7 (11), which indicate that the internal redistribution of pore pressures may significantly modify the actual shape of the isochrones relative to those for the undrained case. To clarify this point and interpret the importance of drainage in liquefaction, the case study shown in Fig. 3 was undertaken. The soil profile is composed of sand with D_r = 45% and a dry unit weight of 1.45 kg/cm^2. The base of the profile was subjected to the random acceleration function proposed by Parmelee et al. (17) scaled to give a maximum acceleration of the order of 0.065 *g*:

$$\ddot{v}_b(t) = 8.9\, t \exp(-0.333t) \sum_{j=1}^{10} \cos(w_j t + \psi_j); \quad t \geq 0 \ldots\ldots\ldots\ldots (15)$$

in which w_j and ψ_j = random circular frequencies and phase angles distributed uniformly in the intervals L and $(0, 2\pi)$, respectively. The computed time history

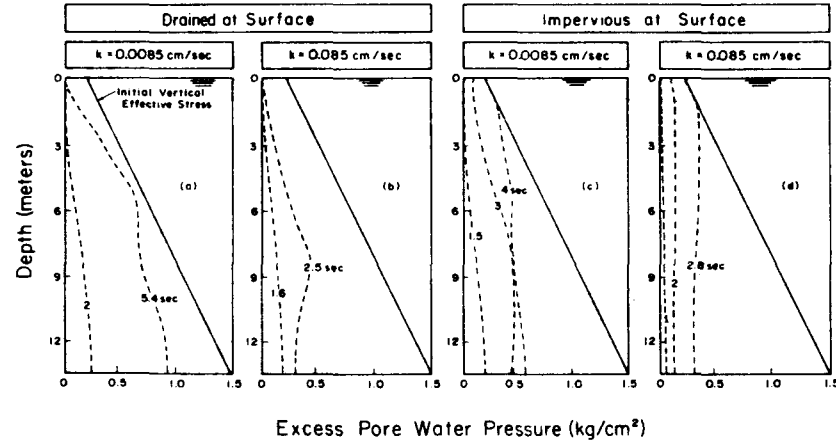

FIG. 4.—Effect of Permeability and External Drainage Conditions on Liquefaction

of the surface acceleration and the pore-pressure increase in the stratum have been determined by assuming that undrained conditions (k = 0) prevail throughout the process. If, on the other hand, redistributions of the pore pressures and free drainage at the top of the layer are allowed to occur, the results shown in Figs. 4(*a*) and 4(*b*) are obtained, depending on the permeability of the sand. The generalized superposition procedure (Eq. 12) has been used for this purpose. In both cases it can be observed that drainage lowers the rate of pore-pressure increase in the deposit to the point that the sand does not liquefy at all under the given earthquake loading (the greater the coefficient of permeability, the greater the decrease). The maximum pore pressures in the layer occur at 5.4 sec at a higher elevation than in the undrained profile; beyond this time, the earthquake motions are such that pore-pressure dissipation takes place faster than pore pressure generation, and the isochrones move away from the initial vertical effective stress line.

If both sides of the deposit are impermeable, the internal redistribution of pore pressures still occurs, but external drainage is prevented. In this case, as shown in Figs. 4(*c*) and 4(*d*), the level of initial liquefaction is raised (practically to the top of the stratum) and the time to liquefaction is decreased (the greater the permeability, the sooner liquefaction occurs). In view of the excellent agreement between the foregoing results and similar data reported by Finn et al. (9), the reason for the contradictory conclusions deduced by Christian (7) may lie in the value of the coefficient of consolidation. The value adopted by Christian to support his arguments (c_v = 1 cm^2/sec) is several orders of magnitude lower than the ones used in this study (c_v = 7,000 cm^2/sec and 70,000 cm^2/sec).

Effect of Soil Compressibility.—The solid curves in Fig. 3 represent the undrained pore-pressure distributions that develop at various times in the profile, as calculated by using data reported by Ansal (1) for the constrained modulus

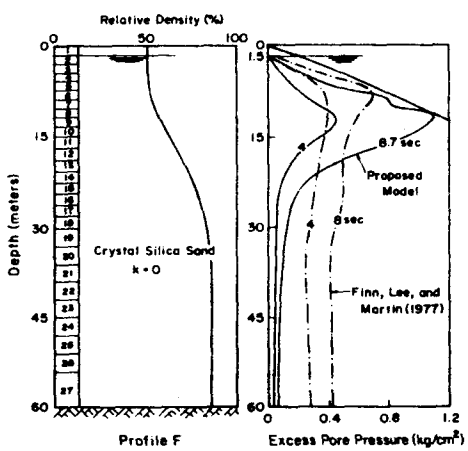

FIG. 5.—Liquefaction of Deep Layer

of compressibility of saturated Crystal Silica No. 20 sand at a relative density of 45%. A direct comparison between these results and the ones obtained by utilizing values provided by others (14) demonstrates that the predictions of liquefaction given by this model are very sensitive to variations in the densification compliance. As pointed out by Seed (19), this vulnerability of analytical methods demands caution in their practical application until the development of good laboratory techniques permits a reliable determination of all the material parameters involved.

Effect of Layer Thickness.—To investigate the effect of layer thickness on liquefaction susceptibility, a 60-m deep layer of undrained sand with a relative density that increases with depth was analyzed. Profile *F* was discretized into 27 finite elements of various lengths and subjected to the same artificial accelerogram considered in the preceding section (Eq. 16). Fig. 5 shows that the sand located at a depth of 11.2 m reached initial liquefaction after 8.7 sec, whereas Finn et al. (9), using the so-called Masing model, have reported

that liquefaction is imminent at a depth of 4.6 m after 8 sec. Thus, the agreement between the predictions of these two inelastic models is excellent, and equally important, these results demonstrate that liquefaction is a phenomenon which occurs primarily at shallow depths (generally less than about 15 m) where the confining pressure is small (10).

Effect of Loading Characteristics.—In principle, the form, frequency, and amplitude of the input motion can affect the liquefaction susceptibility of a sand layer. To evaluate these effects independently a number of loading situations involving profile A have been analyzed. The calculations show (Fig. 6) that, if the amplitude (0.065 *g*) and frequency (2 Hz) of the input motion is held constant, rectangular waves cause the soil to liquefy sooner than either triangular or sinusoidal waves; this result has been obtained in the laboratory by several researchers (12,15). In addition, doubling the amplitude of the sine waves

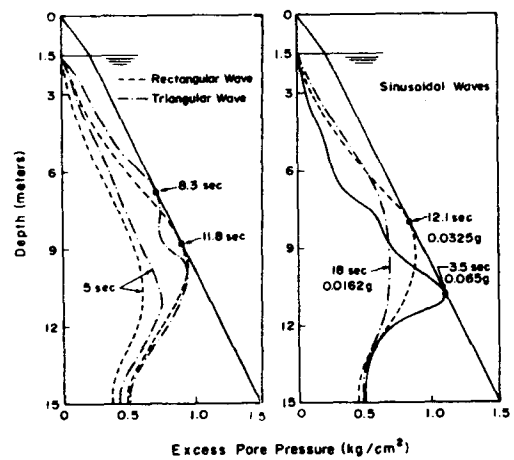

FIG. 6.—Effect of Wave Form and Maximum Acceleration on Development of Excess Pore Water Pressure

drastically shortens the time to liquefaction, the reduction being as much as 70%, depending on the maximum acceleration (Fig. 6).

While these results involve periodic loadings of constant amplitude, a quite different pattern of behavior is obtained for time-varying amplitudes. To investigate the effect of the input motion sequence on liquefaction three different sinusoidal accelerations, all with a frequency of 2 Hz, were applied to profile A. These accelerations were: (1) Linearly decaying; (2) linearly increasing; and (3) random. The maximum amplitude of the oscillation used in the first and third inputs was chosen as the amplitude of the sine curve with f = 2 Hz such that it covered the same area above the positive time axis as the decaying sine curve up to 12.1 sec (time to initial liquefaction of profile A; see Fig. 6). The development of pore pressures in the undrained layer is described in Fig. 7, where the times to liquefaction are found to be 5.9 sec, 8.6 sec, and 9.6 sec, respectively. When the pore pressure histories for the liquefied elements in these three cases are plotted in the same diagram, as done in Fig. 8(*a*),

the relative position of the cycles of base acceleration in a nonuniform cycle sequence conditions the shape of the liquefaction curves in the elements that liquefy. The same trend has been found, both theoretically (14) and experimentally (11), for the effect of nonuniform shear stress cycles on the excess pore pressure buildup in a specimen of saturated sand (Fig. 8).

Thus, it may be concluded that, for fixed-frequency accelerations, the shape and amplitude of the waves, as well as the time-sequence, affect the onset of liquefaction. To establish whether or not the same trends apply to frequency, a parametric study has been conducted with four different time histories of sine wave accelerations, all with the same amplitude (0.0325 g), applied to profile A. The distribution of periods with time and the dynamic isochrones calculated

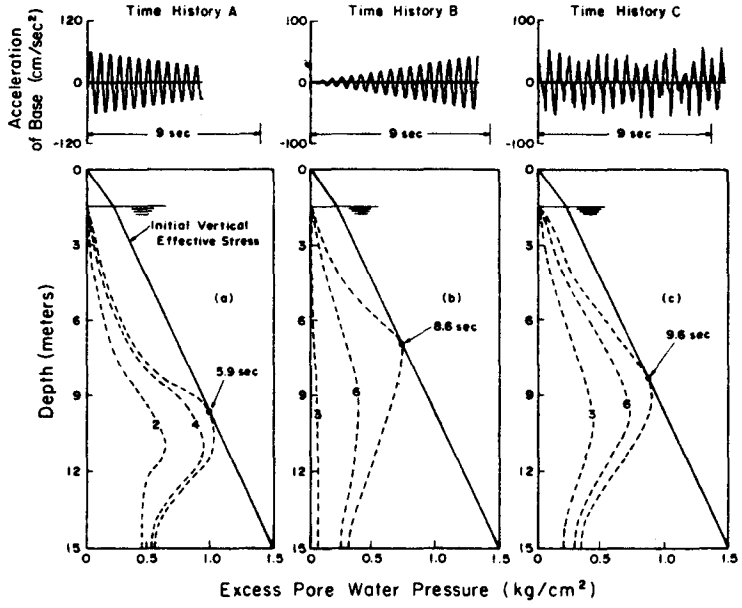

FIG. 7.—Effect of Loading Pattern on Development of Excess Pore Water Pressure

for up to 17 sec of shaking are given in Fig. 9. The computed results seem to indicate that, for narrow band excitations beyond the range of 1 Hz to 2 Hz, the deposit is quite insensitive to liquefaction (this range may vary with the relative density of the sand and the depth of the deposit). On physical grounds it may be expected that inputs having a broad band of decaying frequencies (F) will be more dangerous for a stiffness-degrading material (such as sand) than frequency increasing ones (E), because the progressive softening of the material makes it "tune up" with the tail of the long-period waves arriving at the end of the loading. However, the predictions of the model confirm this behavior only in qualitative trends because, although a higher rate of pore pressure increase is observed for the sequence of decaying frequencies, liquefaction is not achieved in either case after 17 sec of shaking.

Effect of Dynamic Coupling.—Thus far it has been assumed that, since total stresses do not vary with time, Terzaghi's equation of consolidation adequately models the relaxation of pore pressures that occurs simultaneous with the generation process. However, when vertical inertial effects act on the sand deposit, Eq. 7 no longer applies, and the more general framework of Biot's theory of poroelasticity (Eqs. 1 and 5) must be used to obtain the pore pressure response of the stratum. This situation is depicted in Fig. 10, in which the

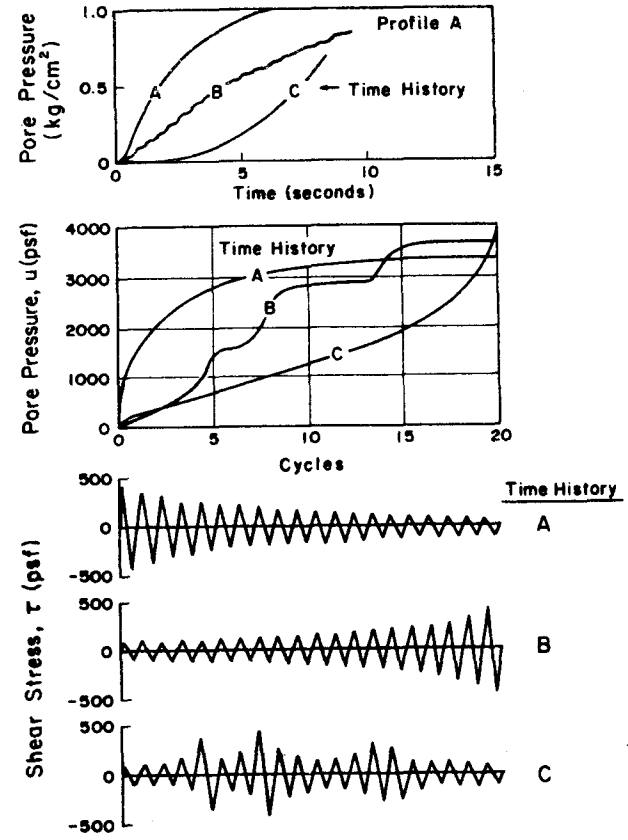

FIG. 8.—Effect of Loading Sequence on Development of Excess Pore Water Pressure: (*a*) Proposed Model; (*b*) After Martin, Finn, and Seed (1975) for Crystal Silica Sand at Relative Density of 45% under Vertical Stress of 4,000 psf

north-south and vertical components of the El Centro accelerogram of May 18, 1940, scaled to a maximum acceleration of 0.1 g, have been applied to a soil column composed of nine 1.5-m finite elements whose relative densities vary with depth in an arbitrary fashion. Since the shear beam model does not account for dilatational waves, a one-dimensional two-phase profile is needed. Although the propagation of compression waves is not really expected to be

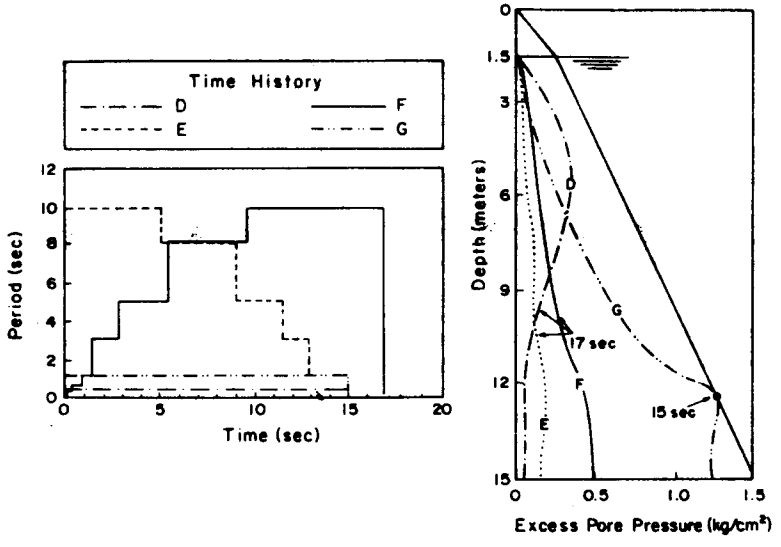

FIG. 9.—Effect of Frequency of Loading on Development of Excess Pore Water Pressure

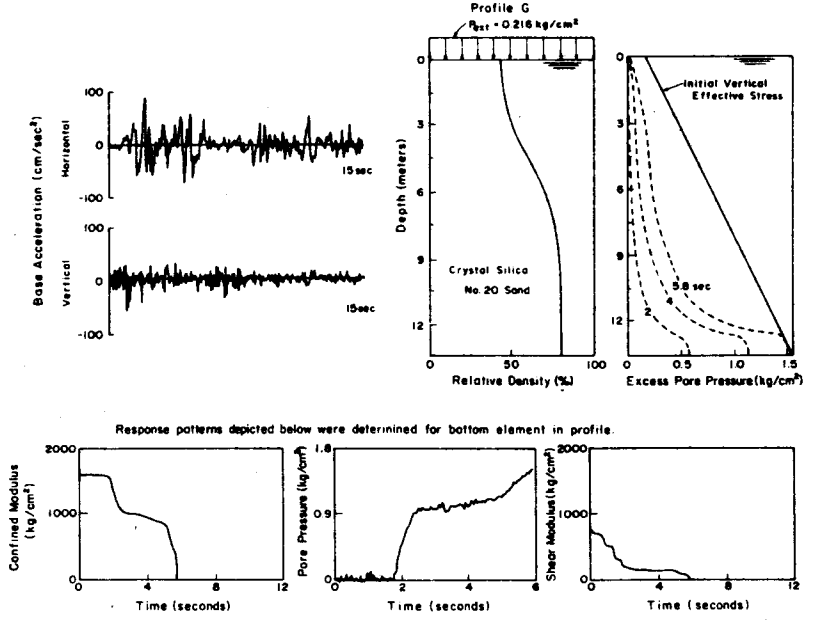

FIG. 10.—Response of Two-phase Layer to Combined Horizontal and Vertical Excitation by Real Accelerogram (Perfect Vertical Coupling)

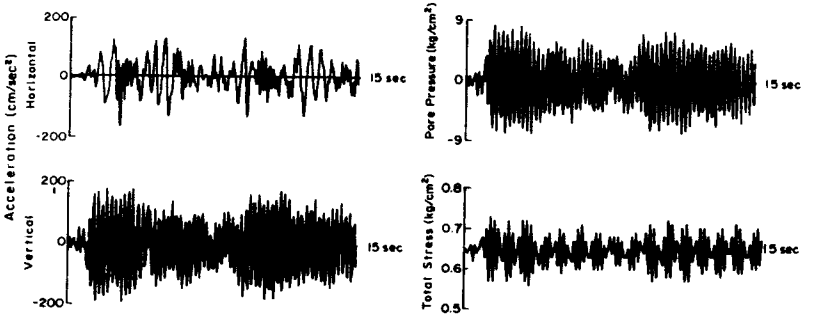

FIG. 11.—Response of Two-phase Layer to Combined Horizontal and Vertical Excitation by Real Accelerogram (Partial Vertical Coupling)

elastic, any more complicated assumption is unjustified because of the lack of data on the dynamic stress-strain relationship in the vertical direction and the inelastic densification of the Crystal Silica sand by pressure waves.

To analyze the influence of different sources of dynamic coupling, two hypothetical situations are considered. First, it is assumed that the vertical motions of the solid and fluid are perfectly coupled ($u = U$); thus, by summing Eqs. 1*a* and 1*b*, the volumetric constitutive equation for the undrained soil becomes $d\sigma_t = d\sigma + d\sigma_F = (M + 2Q + R)\, d\epsilon^{el}$, and only inertial coupling (due to the apparent mass) is taken into account. In this case liquefaction starts at the base of the deposit (Fig. 10) at 5.8 sec. The curve depicting the pore pressure increase in the liquefied element shows an overall monotonic tendency (due to the deviatoric strains) with some superimposed alternating stresses (traction and compression) that emanate from the vertical motions of the column.

On the other hand, Fig. 11 portrays for profile G the situation in which only a partial vertical coupling (due to flow resistance) exists and the two phases do not move together vertically. In this case the effect of viscous damping on the vertical motions (due to the elastic wave propagation, not consolidation) is considered in addition to inertia. The accelerations show that the vertical motions in the solid and fluid phases are approximately the same throughout the profile, the amplification being on the order of 1.3 and 5 for the horizontal and vertical accelerations, respectively, at a depth of 1.5 m below the surface. Also, as a result of the vertical vibration, the dynamic pore water pressure and the total stress (defined at each instant as the sum of the vertical stresses σ and σ_F) merely oscillate around their static values, so that the layer is far from liquefying at 15 sec. Thus, it is conceivable that, in the case of partial vertical coupling, the liquefaction behavior of the stratum is governed entirely by the elastic pressure waves to the extent that no apparent pore pressure buildup due to inelastic densification can be identified. This fact may be of importance in the case of liquefaction by the action of surface (Rayleigh) waves, where horizontal and vertical motions of the soil particles take place simultaneously.

Conclusions

A finite element procedure has been developed to determine the liquefaction

response of a saturated sand deposit subjected to vertically propagating plane waves at its base. The method takes into account the inelastic deviatoric stress-strain relation and the densification characteristics of the sand. Pore pressures are calculated from the volume changes by treating the sand as an inelastic two-phase medium. Analytical estimates of the pore pressure buildup, determined from consolidation theory, are also utilized. Based on the results obtained from a parameter study of site-dependent factors that influence liquefaction, the following conclusions may be advanced:

1. If the unsaturated portion of the soil above the water table is replaced by an equivalent surcharge, the results become more critical as the depth of the water table increases; if the propagation of the shear waves within the unsaturated soil is not considered, the time and depth of initial liquefaction are underestimated and overestimated, respectively.
2. The redistribution of pore pressures due to internal and external seepage conditions raises the zone of liquefaction and influences significantly the liquefaction susceptibility of soil layers; if drainage at the upper boundary is not prevented, the time to liquefaction increases with an increase in the coefficient of permeability, whereas the opposite is found in a stratum that is undrained at the top.
3. Only the upper part of deep layers is capable of liquefying; the looser the sand, the greater its tendency to liquefy.
4. Rectangular acceleration waves produce liquefaction sooner than either triangular or sinusoidal waves; the susceptibility to liquefaction diminishes drastically as the amplitude of the waves decreases and the initial effective confining pressure increases, becoming essentially negligible for frequencies beyond some characteristic band for each deposit.
5. The time rates of pore pressure increases in the liquefied elements are intricately related to the position of the peak in the specified loading sequence; if the peak is located near the end of the bedrock acceleration record, the curve of pore pressure increases with time appears to be convex with respect to the positive time axis, whereas a concave curve is obtained for a load history where the peak occurs near the beginning.
6. Pore pressure distributions that develop at various times in the deposit are very sensitive to the value of the constrained elastic modulus of the sand.
7. The degree of coupling between vertical motions of the solid and fluid has a profound effect on liquefaction in cases where vertical and horizontal accelerations act simultaneously.

Acknowledgment

This study was supported in part by a grant from the National Science Foundation.

Appendix I.—References

1. Ansal, H. K., "Elastic Stress-Strain Behavior of Crystal Silica Sand," thesis presented to Northwestern University, at Evanston, Ill., in 1978, in partial fulfillment of the requirements for the degree of Master of Science.
2. Bažant, Z. P., and Krizek, R. J., "Saturated Sand as an Inelastic Two-Phase Medium," *Journal of the Engineering Mechanics Division,* ASCE, Vol. 101, No. EM4, Proc. Paper 11508, Aug., 1975, pp. 317–332.
3. Bažant, Z. P., and Krizek, R. J., "Endochronic Constitutive Law for Liquefaction of Sand," *Journal of the Engineering Mechanics Division,* ASCE, Vol. 102, No. EM2, Proc. Paper 12036, Apr., 1976, pp. 225–238.
4. Belytschko, T., and Schoeberle, D. F., "On the Unconditional Stability of an Implicit Algorithm for Nonlinear Structural Dynamics," *Journal of Applied Mechanics,* Vol. 42, No. 4, 1975, pp. 465–469.
5. Biot, M. A., "Theory of Propagation of Elastic Waves in Fluid-Saturated Porous Solid—I. Low-Frequency Range," *Journal of the Acoustical Society of America,* Vol. 28, 1956, pp. 168–178.
6. Carslaw, H. S., and Jaeger, J. C., *The Conduction of Heat in Solids,* 2nd ed., Clarendon Press, New York, N.Y., 1959.
7. Christian, J. T., "Consolidation with Internal Pressure Generation," *Journal of the Geotechnical Engineering Division,* ASCE, Vol. 102, No. GT10, Proc. Paper 12445, Oct., 1976, pp. 1111–1115.
8. Cuéllar, V., Bažant, Z. P., Krizek, R. J., and Silver, M. L., "Densification and Hysteresis of Sand under Cyclic Shear," *Journal of the Geotechnical Engineering Division,* ASCE, Vol. 103, No. GT5, Proc. Paper 12908, May, 1977, pp. 399–416.
9. Finn, W. D. L., Lee, K. W., and Martin, G. R., "An Effective Stress Model for Liquefaction," *Journal of the Geotechnical Engineering Division,* ASCE, Vol. 103, No. GT6, Proc. Paper 13008, June, 1977, pp. 517–533.
10. Florin, V. A., and Ivanov, P. L., "Liquefaction of Sandy Soils," *Proceedings of the Fifth International Conference on Soil Mechanics and Foundation Engineering,* Vol. I, International Society of Soil Mechanics and Foundation Engineering, Paris, France, 1961, pp. 107–111.
11. Ishihara, K., and Yasuda, S., "Sand Liquefaction Due to Irregular Excitation," *Soils and Foundations,* Vol. 12, No. 3, Tokyo, Japan, June, 1972, pp. 19–39.
12. Lee, K. L., and Fitton, J. A., "Factors Affecting the Cyclic Loading Strength of Soil," *Vibration Effects on Soils and Foundations,* STP450, American Society for Testing and Materials, Philadelphia, Pa., 1968.
13. Lee, L., and Seed, H. B., "Cyclic Stress Conditions Causing Liquefaction of Sand," *Journal of the Soil Mechanics and Foundations Division,* ASCE, Vol. 93, No. SM1, Proc. Paper 5058, Jan., 1967, pp. 47–70.
14. Martin, G. R., Finn, W. D. L., and Seed, H. B., "Fundamentals of Liquefaction Under Cyclic Loading," *Journal of the Geotechnical Engineering Division,* ASCE, Vol. 101, No. GT5, Proc. Paper 11284, May, 1975, pp. 423–438.
15. Mulilis, J. P., Townsend, F. C., and Horr, R. C., "Triaxial Testing Techniques and Sand Liquefaction," *Dynamic Geotechnical Testing,* ASTM STP654, American Society for Testing and Materials, Philadelphia, Pa., 1978, pp. 265–279.
16. Oh-Oka, H., "Drained and Undrained Stress-Strain Behavior of Sands Subjected to Cyclic Shear Stress under Nearly Plane Strain Conditions," *Soils and Foundations,* Vol. 16, No. 3, Tokyo, Japan, June, 1976, pp. 19–31.
17. Parmelee, R. A., Perelman, D. S., Lee, S. L., and Keer, L. M., "Seismic Response of Structure-Foundation System," *Journal of the Engineering Mechanics Division,* ASCE, Vol. 94, No. EM6, Proc. Paper 6264, Dec., 1968, pp. 1295–1315.
18. Prakash, S., and Gupta, M. K., "Liquefaction and Settlement Characteristics of Loose Sands under Vibrations," *Proceedings of the Conference on Dynamic Waves in Civil Engineering,* Wiley-Interscience, John Wiley and Sons, London, England, 1970, pp. 229–244.
19. Seed, H. B., "Evaluation of Soil Liquefaction Effects on Level Ground during Earthquakes," presented at the October, 1976, ASCE Specialty Conference on Liquefaction Problems in Geotechnical Engineering, held at Philadelphia, Pa. (Preprint 2752).
20. Taylor, D. W., *Fundamentals of Soil Mechanics,* 7th ed., John Wiley and Sons, Inc., New York, N.Y., 1954.

Appendix II.—Notation

The following symbols are used in this paper:

A = compliance function;
b = flow resistance coefficient;
C_d = densification compliance;
C_w = compressibility of water;
c = densification-hardening function (Eq. [2*a*]);
c_v = coefficient of consolidation;
D_r = relative density;
e_{ij} = deviator of strain tensor;
e''_{ij} = deviator of inelastic strain tensor;
F = strain-softening function (Eq. [2*b*]);
G = shear modulus;
g = acceleration of gravity;
H = thickness of deposit;
k = coefficient of permeability;
M, Q, R = volumetric (tangent) elastic moduli;
n = porosity;
p_w = pore water pressure;
p^g_w = excess pore pressure generated in undrained conditions;
s_{ij} = deviator of stress tensor;
t = time;
u, U = vertical displacements in solid and fluid phases;
$\ddot{u}_b, \ddot{v}_b$ = vertical and horizontal bedrock accelerations;
Z_1 = constant in Eqs. 3 and 4;
α, β = parameters of Newmark operator;
γ = shear angle;
γ'' = inelastic shear angle;
γ_w = unit weight of water;
ϵ, ϵ_F = volumetric strains of solid and fluid phases;
ϵ'', ϵ''_F = inelastic strains in solid and fluid phases;
ϵ^{el} = volumetric elastic strain of solid phase;
κ = densification measure (Eq. [2*a*]);
ξ = rearrangement measure (Eq. [2*b*]);
ρ_a = apparent mass density;
ρ_1, ρ_2 = mass densities in solid and fluid phases;
σ, σ_F = volumetric stresses in solid and fluid phases;
σ' = effective stress;
σ_{ij} = stress tensor;
σ_t = total stress ($\sigma + \sigma_F$);
τ = engineering shear stress;
τ = time variable;
ω_j = circular frequency (Eq. 15); and
ψ_j = phase angle (Eq. 15).